Electrostatic Partitioning in Slit Pores by Gibbs Ensemble Monte Carlo Simulation

Myung-Suk Chun and Ronald J. Phillips
Dept. of Chemical Engineering and Materials Science, University of California at Davis, Davis, CA 95616

Equilibrium partitioning of spherical solutes between slit pores and bulk solution is investigated by the Gibbs ensemble Monte Carlo method. Two types of perturbations are performed in this simulation: a random displacement of solutes that ensures equilibrium within both bulk and pore regions, and random interchanges of solutes that equalize the interaction potentials between the two regions. To study the effects of electrostatic interactions, interaction energies between the solutes and pore walls and between pairs of solutes are evaluated by using a singularity method. Partition coefficients calculated for neutral solutes, which experience purely steric interactions, increase with increasing solute concentration and agree well with existing theoretical results. For pores and solutes of like charge, results for the limit of infinitely dilute solute concentration show a sharp decline in partition coefficient with decreasing ionic strength of solution. As the solute concentration increases, the interplay of solute–wall and solute–solute interactions becomes increasingly important, and the partition coefficient increases accordingly. The density profiles indicate unambiguously that, whether solutes and pores are uncharged or of like charge, solute–solute interaction promotes enhanced concentrations near the wall, causing the partition coefficient to increase. Even at solute concentrations as low as 5%, effects of solute–solute interactions caused by electrostatic charge can more than compensate for sphere–wall repulsive interactions, indicating that concentration effects should be considered at least as important as electrostatic effects in partitioning phenomena.

Introduction

The equilibrium partitioning between a bulk solution and an adjacent porous solid is an important aspect of hindered diffusion (Deen, 1987), solute transport, and a number of related separation processes such as membrane filtration and size-exclusion chromatography (Yau et al., 1979; Edwards and Dubin, 1993). The macroscopic property describing this phenomenon is the partition coefficient K, defined as the ratio of mean pore-to-bulk concentration at equilibrium, or C_p/C_b. In the limit of very dilute concentration, the partition coefficient for charged spherical solutes within slit pores can be expressed by

$$K = \frac{C_p}{C_b} = \int_0^{1-\lambda} e^{-E(z)/kT}\, dz, \tag{1}$$

where the potential energy function $E(z)/kT$ consists largely of contributions from long-range electrostatic repulsion between the solute and the pore wall. These repulsive interactions depend on the solute-to-wall separation z, and also on λ, which is the ratio of the solute diameter d to the pore width D. In Eq. 1 the distance z is made dimensionless by the pore width D. If only uncharged solutes are present in a neutral pore, then purely steric, hard-sphere–hard-wall interactions determine the partition coefficient in the dilute limit. In that case, Eq. 1 reduces to

$$K = 1 - \lambda. \tag{2}$$

Determining how solute concentration affects the partition coefficient is an interesting and significant problem. Glandt (1981) and Anderson and Brannon (1981) have performed statistical thermodynamic analyses of the concentration ef-

Correspondence concerning this article should be addressed to R. J. Phillips.

fect in slit and cylindrical pores to derive a virial expansion for the partition coefficient K, and give results for uncharged spherical solutes. Post (1989) calculated the effect of solute concentration at concentrations where the virial expansions are not expected to be accurate by using linear density functional theory. Like Glandt (1981) and Anderson and Brannon (1981), he considered uncharged spherical solutes in both slit and cylindrical pores. Recently, Pospisil et al. (1993) have used integral equation theory to obtain density profiles and partition coefficients for hard spheres confined within slit pores of varying dimensions over a wide range of bulk concentrations.

The effects of electrostatic interactions on the partitioning of charged colloids in the limit of very dilute solute concentration are discussed briefly by Anderson and Brannon (1981), and are analyzed in detail in the context of cylindrical pores by Smith and Deen (1983) and Mitchell and Deen (1984). Smith and Deen (1983) obtained the electrostatic potential by solution of the linearized Poisson-Boltzmann equation, and thereby derived analytical expressions for the interaction energy of spherical solutes having constant surface potential or surface charge density. Mitchell and Deen (1984) extended the analysis to partitioning in cylindrical pores at low but finite solute concentrations by evaluating the second virial coefficient. They found that the partition coefficient increases with increasing solute concentration. To date, results for electrostatic partitioning in slit pores have not been published either in the limit of infinite dilution or at moderate solute concentrations.

For nondilute solute concentrations, or when the pores of interest have geometries more complicated than the cylindrical and slit pores discussed above, modeling partitioning behavior by using virial expansions or density functional theory is more difficult. As one might expect, these difficulties associated with complicated geometry become even more severe when colloidal interactions cannot be neglected. In such situations, Monte Carlo techniques, of which the grand canonical Monte Carlo (GCMC) method has been most prominent, have been found to be very useful. MacElroy and Suh (1986, 1987) computed partition coefficients for hard spheres in cylindrical pores by using GCMC simulations, and compared their results with the relevant theoretical expressions and with experimental data. The GCMC simulation has also been applied to the partitioning of hard spherical solutes within disordered porous solids such as sponge-like matrices (Fanti and Glandt, 1989). Post and Kofke (1992) have considered the partitioning of fluids sterically confined to narrow pores with adsorbing walls by using a low-dimensional approach that compared favorably with GCMC simulations results.

In the present study, the effect of electrostatic interactions on the partitioning of spherical solutes within slit pores is explored by using the Gibbs ensemble Monte Carlo (GEMC) method. This approach has been used previously with considerable success to study problems of equilibria between phases and between bulk fluids and porous media (Panagiotopoulos, 1987; de Pablo and Prausnitz, 1989; Lastoskie et al., 1993; Green et al., 1994). Panagiotopoulos (1987) employed the GEMC method to study condensation in cylindrical pores in equilibrium with a bulk phase, and Panagiotopoulos et al. (1988) have suggested the possibility of applying it to the study of membrane partitioning. However, this method has not yet been used to study the effects of the screened electrostatic interactions that play a major role in physicochemical problems involving aqueous colloidal suspensions. In this work, both wall-particle and particle-particle energy profiles are determined by using the method recently described by Phillips (1995), which provides accurate solutions to the linearized Poisson-Boltzmann equation. Partition coefficients are evaluated for both charged and uncharged systems for a wide range of ratios of solute diameter to pore width (i.e., $0 < \lambda < 0.86$). For charged systems, ionic strengths of 1, 10, and 100 mM are considered. Our simulation results are compared with results from the literature and with results we have calculated by performing virial expansions.

Gibbs Ensemble Monte Carlo Simulations for Equilibrium Partitioning

The GEMC method allows one to simulate coexisting subsystems consisting of a pore region p and a bulk region b in equilibrium at a temperature T. To achieve this end, pore and bulk regions are constructed having volumes V_p and V_b and containing N_p and N_b solute particles, respectively, with the total number of particles N being the sum of N_p and N_b. In the GEMC method, the two regions are allowed to interchange particles and the volumes are allowed to fluctuate in order to satisfy the equilibrium conditions of the temperature, pressure, and chemical potential μ (Panagiotopoulos et al., 1988). In essence, elements of canonical (NVT), isobaric-isothermal (NPT), and grand canonical (μVT) ensembles are combined in the Gibbs ensemble, so a computation cycle generally consists of three types of moves in a GEMC simulation. However, in our pore-bulk system there is no need to include exchanges of volume between the two regions, because the condition for mechanical equilibrium is automatically satisfied if the chemical potentials in each region are equal (Lastoskie et al., 1993). Therefore, only particle displacement and interchange moves are performed. This fact represents an attractive feature of the GEMC method in simulations of this type. A readable and detailed description of the GEMC method can be found in the article by Green et al. (1994).

As described in Figure 1, the first type of move involves the random displacement of particles in each subsystem. In this stage, the particles are chosen and displaced randomly within the periodic unit cells following the NVT Metropolis scheme (Allen and Tildesley, 1987). States in the canonical NVT ensemble occur with a probability proportional to $\exp(-E^{\alpha}/kT)$ for an arbitrary subsystem α, where kT is the Boltzmann thermal energy. The new configurations of subsystem α are thus generated with a probability $\mathcal{P}_D$ given by

$$\mathcal{P}_D = \min\left[1, \exp\left(-\frac{\Delta E^{\alpha}}{kT}\right)\right], \tag{3}$$

where ΔE^{α} ($= E^{\alpha}_{\text{new}} - E^{\alpha}_{\text{old}}$) represents the change in interaction energy in subsystem α caused by the move. If purely steric interactions are involved, the solute-solute pair potential energy is expressed as

$$\begin{aligned} E_{s-s}(h) &= \infty \quad h < d \\ &= 0 \quad h > d. \end{aligned} \tag{4}$$

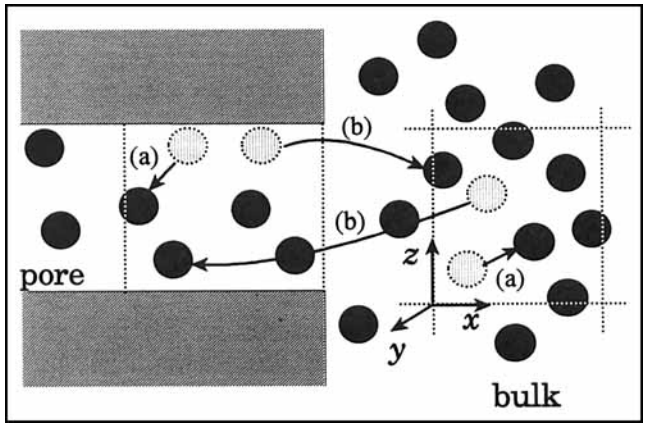

Figure 1. GEMC method for the simulation of equilibrium partitioning.

Dotted lines indicate periodic boundary conditions. Each cycle consists of (a) random particle displacements in each region and (b) particle interchange between the two regions.

Similarly, the potential energy between solute and pore wall is given by

$$E_{s-w}(h) = \infty \qquad h < d/2$$
$$= 0 \qquad h > d/2, \tag{5}$$

where h corresponds either to the separation distance between two solutes or between the solute and the pore wall, and the solute of diameter d is confined within the pore walls separated by the pore width D.

The second type of move is a particle interchange between regions α and β, which is similar to the particle creation and annihilation in the grand canonical μVT ensemble scheme. In the case of particle creation in subsystem α, the ratio of the probabilities of the new and old states is

$$\mathcal{P}_T^{\alpha} = \exp\left[\ln\left(\frac{\Lambda V^{\alpha}}{N^{\alpha}+1}\right) - \frac{\Delta E^{\alpha}}{kT}\right], \tag{6}$$

where Λ is the de Broglie wavelength and V^{α} and N^{α} are the volume and number of particles in subsystem α, respectively. The total number of particles in the whole system is conserved, so a simultaneous trial move in subsystem β involves an attempted particle destruction with the ratio of probabilities given as

$$\mathcal{P}_T^{\beta} = \exp\left[\ln\left(\frac{N^{\beta}}{\Lambda V^{\beta}}\right) - \frac{\Delta E^{\beta}}{kT}\right], \tag{7}$$

where the superscript β indicates that the quantities N, V, and E are calculated for subsystem β. The probability governing the transfer of a particle from subsystem α to subsystem β is obtained by combining Eqs. 6 and 7, yielding the final result

$$\mathcal{P}_T = \min\left[1, \exp\left\{\ln\left(\frac{N^{\alpha}V^{\beta}}{(N^{\beta}+1)V^{\alpha}}\right) - \frac{\Delta E^{\alpha}+\Delta E^{\beta}}{kT}\right\}\right]. \tag{8}$$

Note that the number of particles in each subsystem fluctuates due to the particle transfer. Unlike the cases of NVT and NPT simulations, the probability of choosing a particular particle changes during a GEMC simulation.

Electrostatic interaction energy

When the solutes and the pore walls are charged, electrostatic interactions contribute to the energy E in Eqs. 3 and 8. Here these electrostatic interaction energies are calculated by using the linearized Poisson–Boltzmann equation, which is given by

$$\nabla^2\psi = (\kappa a)^2\psi, \tag{9}$$

where the electrostatic potential ψ is made dimensionless by a characteristic surface potential, the Laplacian operator ∇^2 is made dimensionless by using the solute radius a, and κa is the dimensionless, inverse Debye length. For aqueous solutions of 1-1 electrolytes at 25°C, the inverse Debye length κ is given by (Hunter, 1989)

$$\kappa(\mathrm{nm}^{-1}) = 3.278\sqrt{I(M)}, \tag{10}$$

where I denotes the ionic strength of the solution. In solving Eq. 9, we assume the solute and pore surfaces S have a constant surface-charge density σ, leading to the boundary condition

$$\mathbf{n}\cdot\nabla\psi = \sigma \qquad \text{on } S, \tag{11}$$

where $\mathbf{n}$ is a unit normal vector pointing into the solvent.

For electrostatic interactions between surfaces with potentials comparable to or lower than the thermal potential kT/e, where e is the elementary electrostatic charge, it has been shown by direct calculation that the linearized Poisson–Boltzmann equation provides a good approximation to its nonlinear counterpart (Carnie et al., 1994). Inaccuracies in the linearized Poisson–Boltzmann equation with constant charge boundary conditions occur only at surface separations so small as to be rendered highly improbable because of the associated high interaction energies. Similarly, recent theoretical work in statistical mechanics shows that the Poisson–Boltzmann equation is a legitimate, limiting case of the three-point extension of the hypernetted chain/mean-sphere approximation (TPE-HNC/MS) (Lozada-Cassou and Diaz-Herrera, 1990a,b) at low to moderate surface potentials and low ionic strengths. The TPE-HNC/MS is an integral equation theory in which ion–ion interactions are treated by using the mean-sphere approximation, and ion–wall or ion–particle interactions are calculated by using the hypernetted chain approximation. Hence, even though the linearized Poisson–Boltzmann equation accounts for the ions in solution in an averaged sense, the energetic interactions used in this work should correspond at least qualitatively, and in some cases quantitatively, to those one would obtain by more rigorous Monte Carlo or integral equation approaches in which the ions are explicitly taken into account.

We solve Eq. 9 subject to the boundary condition in Eq. 11 by using a singularity method described previously (Phillips,

1995). This method is very similar to that described by Dabros (1985) for use in low-Reynolds-number hydrodynamics problems. Essentially, the solution is found as a sum of contributions from point charges located inside the solute and solid wall. The strengths of the singularities are found by minimizing the deviation from the prescribed boundary conditions at a finite number of points on the surfaces of the solids. The minimization is performed by using the Double-Precision Least-Squares Regression Routine (DLSQRR) in the Integrated Mathematics Subroutines Library (IMSL), as described by Phillips (1995). Once the solution for the potential ψ is obtained, the force can be calculated from

$$\boldsymbol{F} = \int_S \boldsymbol{T} \cdot \boldsymbol{n} dS. \tag{12}$$

Here the Maxwell stress tensor **T** is given by

$$T = \left(\Pi + \frac{1}{2}\epsilon \boldsymbol{E} \cdot \boldsymbol{E}\right) \boldsymbol{I} - \epsilon \boldsymbol{E}\boldsymbol{E}, \tag{13}$$

where ϵ is the dielectric constant, $\boldsymbol{I}$ is the identity tensor, $\boldsymbol{E}$ is the electric field given by $\boldsymbol{E} = -\nabla\psi$, and Π is the osmotic pressure, which is related to the electrostatic potential by

$$\Pi = \frac{1}{2}\epsilon\kappa^2\psi^2. \tag{14}$$

Once the force on the sphere is known, the particle–particle and particle–wall energy profiles can be obtained by simply integrating according to

$$E(h) = \int_{-\infty}^{h} F_z dz = \int_{-\infty}^{h} \left[\boldsymbol{e}_z \cdot \int_S \boldsymbol{T} \cdot \boldsymbol{n} dS \right] dz, \tag{15}$$

where $-\infty$ indicates a sphere–wall separation large enough so that any electrostatic interaction is negligible, in this case taken to be 15 Debye lengths. We note that, for solutions to the linearized Poisson–Boltzmann equation, the energy itself can be calculated directly in terms of surface integrals (Smith and Deen, 1983). However, inasmuch as that would require integrating over the unbounded wall surface, in this case it is simpler to integrate the force over the separation distance. Plotted in Figures 2a and 2b are sphere–sphere and sphere–wall interaction energies normalized by $\epsilon(kT/e)^2 a$. From Eq. 10, one finds that the κa values given correspond to ionic strengths ranging from 0.1 mM to 0.1 M for a solute with a radius of 20 nm.

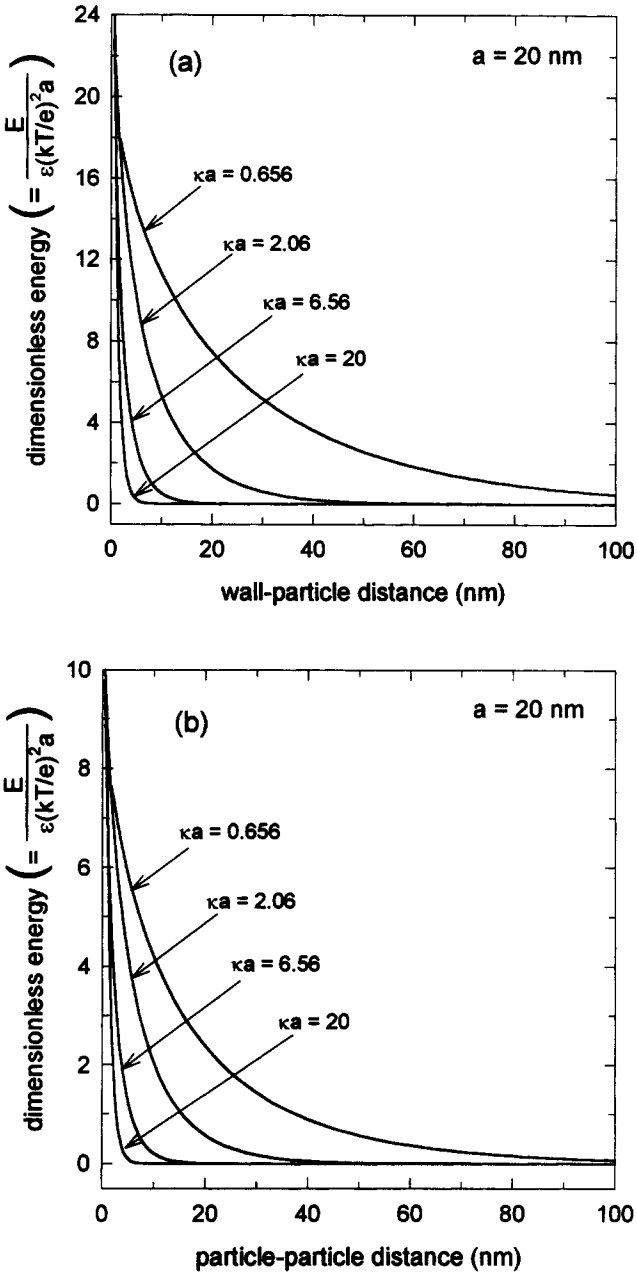

Figure 2. Dimensionless energy profiles for (a) wall–particle and (b) particle–particle interactions for several inverse Debye lengths with constant surface-charge boundary conditions.

Computational method

General descriptions of the procedure for GEMC simulations can be found in the earlier works of Panagiotopoulos (1987) and Panagiotopoulos et al. (1988). One cycle in our simulations consists of N_p and N_b trial displacements in the pore and bulk subsystems, respectively, and N_t trial particle transfers between those two regions. A sufficiently large number of solute particles (usually 500–1,300) is used to ensure that the results are independent of system size, and for an initial condition we use particles arranged in face-centered cubic (FCC) lattices in the two separate regions. Periodic boundary conditions are imposed in the slit pore for both the x and y directions (i.e., the directions parallel to the walls), and the pore walls are located at $z = 0$ and $z = D$. The solute radius a is held constant at 20 nm, and the pore width D is varied to achieve different values of the ratio $\lambda = 2a/D$. In the bulk region, periodic boundary conditions are applied in all directions, as illustrated in Figure 1. Consequently, whereas the periodic unit cell of the bulk region is always a cube, the unit cell of the pore region is rectangular in shape.

For the particle displacements, the sizes of the random steps in the three coordinate directions are chosen to be 50%

of the corresponding dimension of the periodic unit cell. New configurations generated by the particle displacements and the particle transfers are accepted with probabilities given by Eqs. 3 and 8. To determine whether or not to accept a new configuration, a random number between 0 and 1 is generated, and the respective moves are accepted if the random number is less than the computed probability. The number of particle transfers is chosen so that between 4 and 8% of the number of particles in each region are transferred successfully in each cycle; typically 30–40% of transfers are successful at the higher bulk concentrations (i.e., $C_b = 20.9\%$) and smaller pore widths, while 70–80% are successful at the lower concentrations and larger pore widths. Our simulations typically require from $2\text{–}4\times10^4$ configurations to reach equilibrium, and discarding the nonequilibrium configurations, the averages are accumulated over an additional $4\text{–}20\times10^4$ production configurations. All of our simulations were carried out on a Hewlett-Packard 9000 715/100 workstation.

In Figures 3a and 3b, we demonstrate a typical plot of the partition coefficient K as a simulation proceeds with only steric interactions. The values of K shown are calculated from "blocks" of configurations with lengths equal to 1/50th of the total simulation. The representative CPU time requirement is also provided. For the simulation in Figure 3, the concentration of solute in the bulk at equilibrium is 10.5% by volume, the ratio λ is 0.2, and systems with total numbers of particles equal to 540 and 1,088 are considered. One sees that the partition coefficient rapidly converges to a well-defined equilibrium value. In general, the partition coefficient calculated by using smaller numbers of particles fluctuates somewhat more than that for systems with larger numbers of particles.

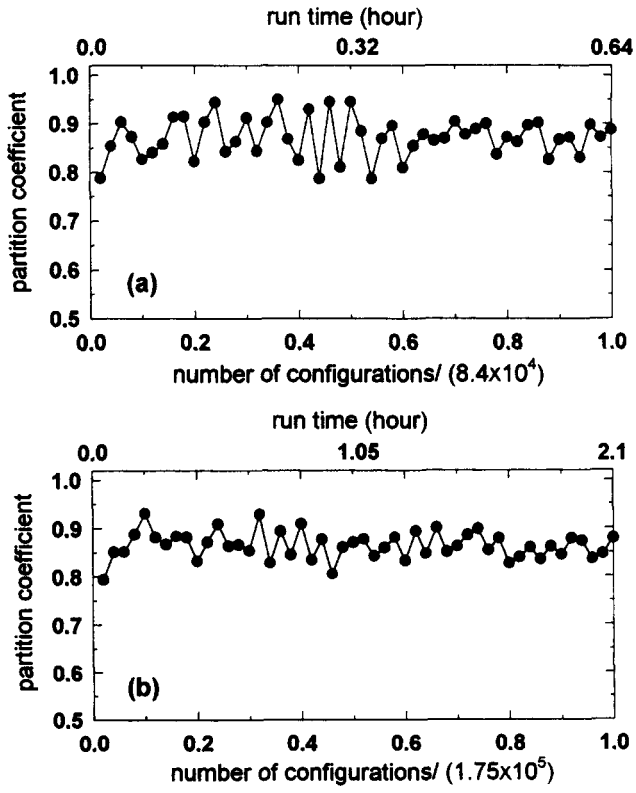

Figure 3. Partition coefficients (steric interactions only) calculated for " blocks" of configurations with lengths equal to 1/50th of the total simulation vs. number of configurations generated for a GEMC simulation.

Solute concentration $C_b = 10.5\%$, $\lambda = 0.2$; (a) $N = 540$ ($N_b = 216$, $N_p = 324$) and (b) $N = 1{,}088$ ($N_b = 512$, $N_p = 576$).

For the partition problem with electrostatic interactions, the total energies of both regions after the particle displacements and interchanges are evaluated by using a pairwise additivity assumption with respect to the wall–particle and particle–particle interactions. Phillips (1995) showed that the pairwise additivity approximation is accurate for such interactions when the particle radius is larger than the Debye length (i.e., $\kappa a > 1$). At separations where electrostatic interaction is almost negligible (i.e., $E(z)/kT \le 10^{-5}$), E/kT is set to zero, yielding a Boltzmann factor of unity. The interaction energy at other particle–particle or particle–wall separation distances is determined by interpolating with Newton–Gregory forward polynomials (Gerald and Wheatley, 1992). The number of tabulated points for the interpolation ranged from 20 to 36, and interpolation with a polynomial of degree 7 is sufficient to yield accurate results. This approach of interpolating with polynomials was checked by comparing with fitted energy profiles that decay exponentially with the separation h as

$$E(h) = \sum_{j=1}^{2} A_{1,j} \exp(-A_{2,j} h), \tag{16}$$

a form that is based on that used by Smith and Deen (1983). The coefficients $A_{1,j}$ and $A_{2,j}$ are determined by regression, and are functions of the Debye length and surface-charge density. Partition coefficients obtained using the polynomial interpolation described above and those obtained using Eq. 16 differ by less than 4%. The computation time for GEMC simulations that include electrostatic interactions is increased significantly over the uncharged case, and was typically approximately 30 CPU hours.

Virial expansion

For purposes of comparison, we have also computed the partition coefficient by using the virial expansion method, which is valid at low volume fractions. The partition coefficient K can be expressed in terms of the bulk volume fraction C_b as

$$K = K_0 + K_1 C_b + \cdots, \tag{17}$$

where K_0 and K_1 are the first and second virial coefficients, respectively. Following Glandt (1980, 1981), these coefficients are obtained by integrating the solute density profiles $\rho(z)$ expressed by

$$\rho(z) = \rho_b e^{-E(z)/kT}(1 + \rho_b Y_1(z) + \cdots), \tag{18}$$

where

$$Y_1(z) = \int (e^{-E(z)/kT} - 1) f(\mathbf{r}, \mathbf{r}_1)\, d\mathbf{r}_1 \tag{19}$$

and the solute number density in the bulk ρ_b is given by

$$\rho_b = \frac{C_b}{(4/3)\pi a^3}. \tag{20}$$

In Eq. 19, one sphere is at position r, a distance z from the wall, and a second sphere is at position r_1. The integral is over all space. The Mayer function $f(r, r_1)$ depends on the solute–solute interaction and is given by

$$f(r, r_1) = e^{-E(r, r_1)/kT} - 1, \tag{21}$$

where the energy profiles are evaluated by the singularity method described above. Hence, the coefficient Y_1 is defined in terms of configuration-space integrals that involve both solute–wall and solute–solute interactions. From Eqs. 17 and 18, one can show that the first virial coefficient K_0 corresponds to the infinite-dilution result given in Eq. 1, sometimes referred to as the Henry's law constant. The second virial coefficient K_1 that accounts for solute concentration effects to leading order is given by

$$K_1 = \int_0^{1-\lambda} (e^{-E(z)/kT}) \frac{Y_1(z)}{(4/3)\pi a^3}\, dz. \tag{22}$$

Simulation Results and Discussion

Partitioning with steric interactions only

In Figure 4, we present results from the GEMC method for the partition coefficient of uncharged systems with solute concentrations in the bulk ranging from infinite dilution to 31.4%. Because bulk concentrations cannot be specified *a priori* in these simulations, the conditions that generate partition coefficients at specified values of C_b are determined by trial-and-error. Earlier results predicted from virial expansions (Glandt, 1981), linear density functional theory (Post, 1989), the two-dimensional approximation (Glandt, 1981; Post, 1989; Post and Kofke, 1992), and semi-grand-canonical Monte Carlo simulations (Post and Kofke, 1992) are also plotted for comparison.

It can be seen that, for bulk solute concentrations of less than 10.9% (i.e., less than 0.2 M), our GEMC results are nearly identical to both those obtained by the virial expansion method and linear density functional theory for values of the ratio λ up to approximately 0.6. For values of λ greater than 0.6, our results agree with the two-dimensional approximation. This agreement is quantitative for concentrations up to nearly 20.9%, and is qualitative at the highest concentration of 31.4% in that both the two-dimensional theory and our simulations show an increase in the partition coefficient as λ increases (i.e., as the pore narrows). The increase in K for $\lambda > 0.5$ can be explained in terms of the development of a two-dimensional, close-packed monolayer of solute within the narrow pore (MacElroy and Suh, 1986). For our simulations at $\lambda > 0.5$ and at a bulk concentration of 31.4%, a very low fraction of particle transfers is successful due to frequent overlap with the pore walls and existing particles, making it difficult to get accurate GEMC results under those conditions. Since the methods of Post and Kofke (1992) did not suffer from this drawback, we believe their results to be the more reliable in that range.

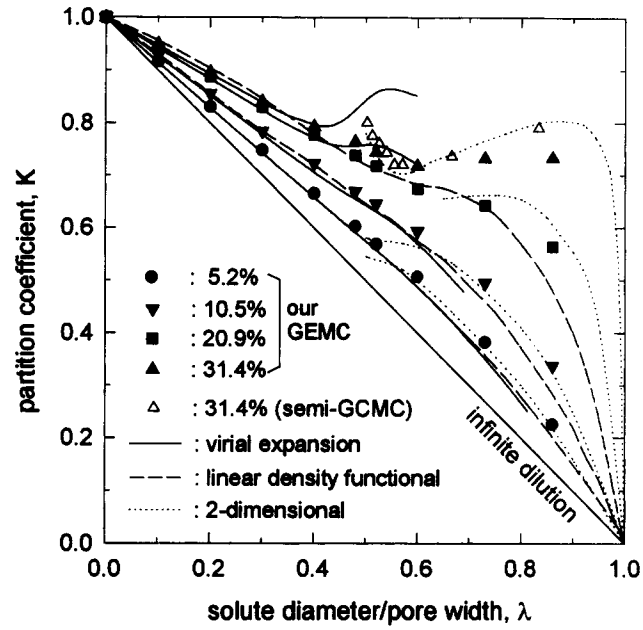

Figure 4. GEMC results for a purely steric partition coefficient K as a function of ratio of solute diameter to pore width λ for various solute concentrations.

For comparison, previous results are provided as follows: virial expansion (—) for $C_b = 5.2$, 10.5, 20.9, and 31.4% (Glandt, 1981); linear density functional theory (---) for $C_b = 5.2$, 10.5, and 20.9% (Post, 1989); two-dimensional approximation (···) for $C_b = 5.2\%$ (Glandt, 1981), 10.5 and 20.9% (Post, 1989), and 31.4% (Post and Kofke, 1992); semi-grand-canonical Monte Carlo simulations for $C_b = 31.4\%$ (Post and Kofke, 1992).

It is also apparent that the virial expansion results become unreliable at the higher concentrations and larger values of λ. Interestingly, for $\lambda < 0.5$ the rate of increase of the partition coefficient with solute concentration is greatly reduced at solute concentrations greater than about 20.9%. This trend is even more apparent in Figure 5, where the data are normalized by the infinite dilution partition coefficient, $K = 1 - \lambda$, and results at concentrations of 20.9% and 31.4% are nearly indistinguishable. The fact that changes in the partition coefficient with changing solute concentration occur so abruptly at low concentrations makes clear the need to exercise caution when neglecting such effects in interpreting experimental data.

The density profile of solutes in the slit pores was monitored in each simulation. Figure 6 illustrates the density profiles across the half-width of a slit pore for which $\lambda = 0.2$ for solute concentrations of 5.2 and 20.9%. The density profiles fluctuate due to the instantaneous sampling used to generate them, in part because the number of particles in each region changes continuously. The density profiles from the simulations are compared with corresponding predictions from the virial expansions of Glandt (1980), and agree well with his results, demonstrating that our simulations are indeed capturing the equilibrium behavior of this system. The fact that the solute density is relatively high near the pore wall is typical of what is seen in equilibrium partitioning of uncharged,

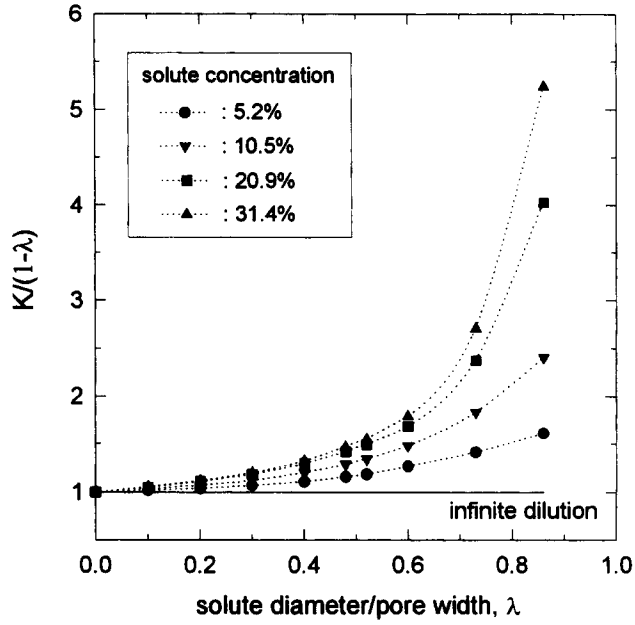

Figure 5. Reduced partition coefficient $K/(1-\lambda)$ vs. ratio of solute diameter to pore width λ with various solute concentrations in the bulk.

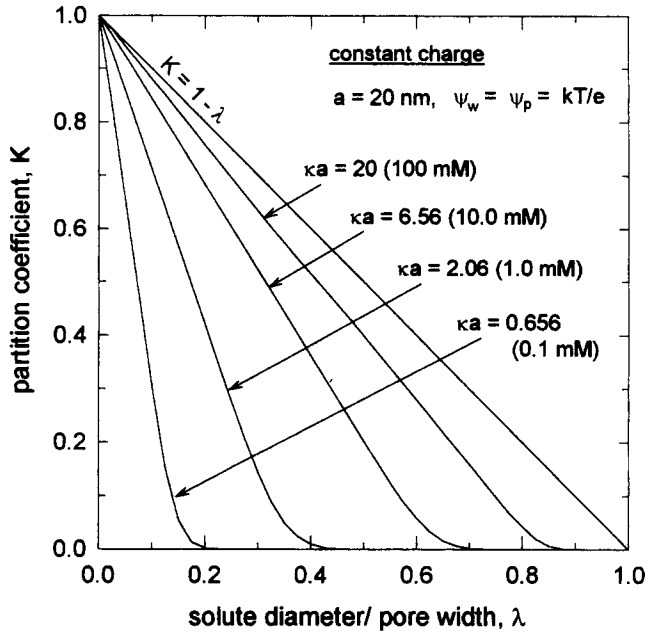

Figure 7. Partition coefficient K at infinite dilution ($C_b = 0$) as a function of λ for several ionic strengths.

spherical solutes, and is discussed further below in the context of our results for charged systems.

Partitioning with electrostatic interactions

The presence of electrostatic interactions affects partitioning behavior in slit pores significantly. Here we consider cases where the solute and pore walls, when they are isolated and not interacting with each other, have surface potentials equal to kT/e, or 25.69 mV. When the solutes and pore walls interact, the surface potentials vary, but the surface-charge densities remain constant in accordance with Eq. 11. In the dilute limit, where solute–solute interactions are negligible, repulsion between the solute and pore walls leads to a sharp decrease in the partition coefficient K. This decrease is shown in Figure 7, where the partition coefficient K is plotted as a function of λ ($= 2a/D$) for a particle with a radius a of 20 nm. These results are calculated by using Eq. 1. Ionic strengths range from 0.1 mM to 100 mM, under which conditions the dimensionless, inverse Debye lengths κa vary from 0.656 to 20, respectively. As κa increases, the partition coefficient approaches the hard-sphere result $1-\lambda$, as one would expect.

When the solute concentration C_b increases, both solute–wall and solute–solute interactions must be considered. Our results for partition coefficients at bulk concentrations up to 20.9% by volume and for λ in the range $0 < \lambda \leq 0.86$ are shown in Figures 8a, 8b, and 8c. Based on calculations from simulation "blocks" such as those shown in Figure 3, the error in these results can be taken to be less than 5%. Results for high ionic strength, where $\kappa a = 20$, are shown in Figure 8a, where they are compared with corresponding results for the uncharged case. Clearly, the effect of solute concentration, which is significant in the uncharged case, is even more so in the presence of repulsive electrostatic interactions. Even at a bulk concentration of 5.2%, solute–solute interactions increase the partition coefficient to a value higher than the value of $1-\lambda$ predicted for hard spheres at infinite dilution. At bulk concentrations of 10.5% and above, there is little difference between the partition coefficient for the charged and uncharged systems, even at the highest values of λ.

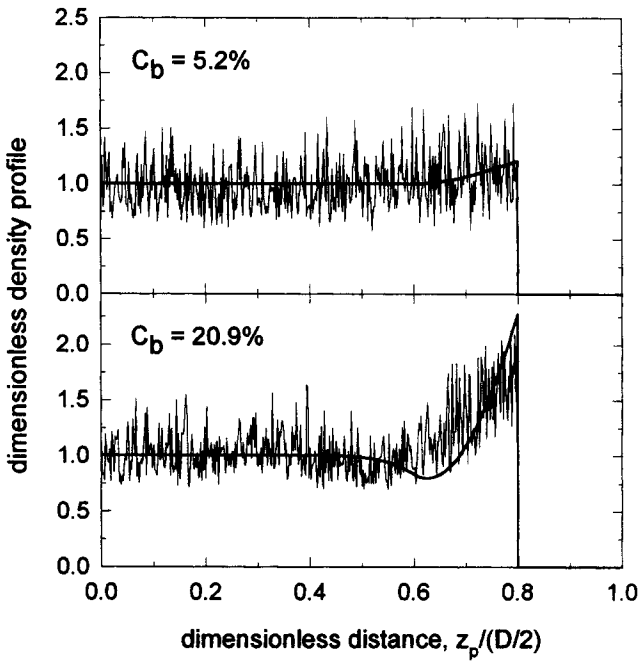

Figure 6. Density profile of uncharged solutes in the pore for $\lambda = 0.2$ and solute concentrations of 5.2 and 20.9%.

Solid curves correspond to virial expansion results.

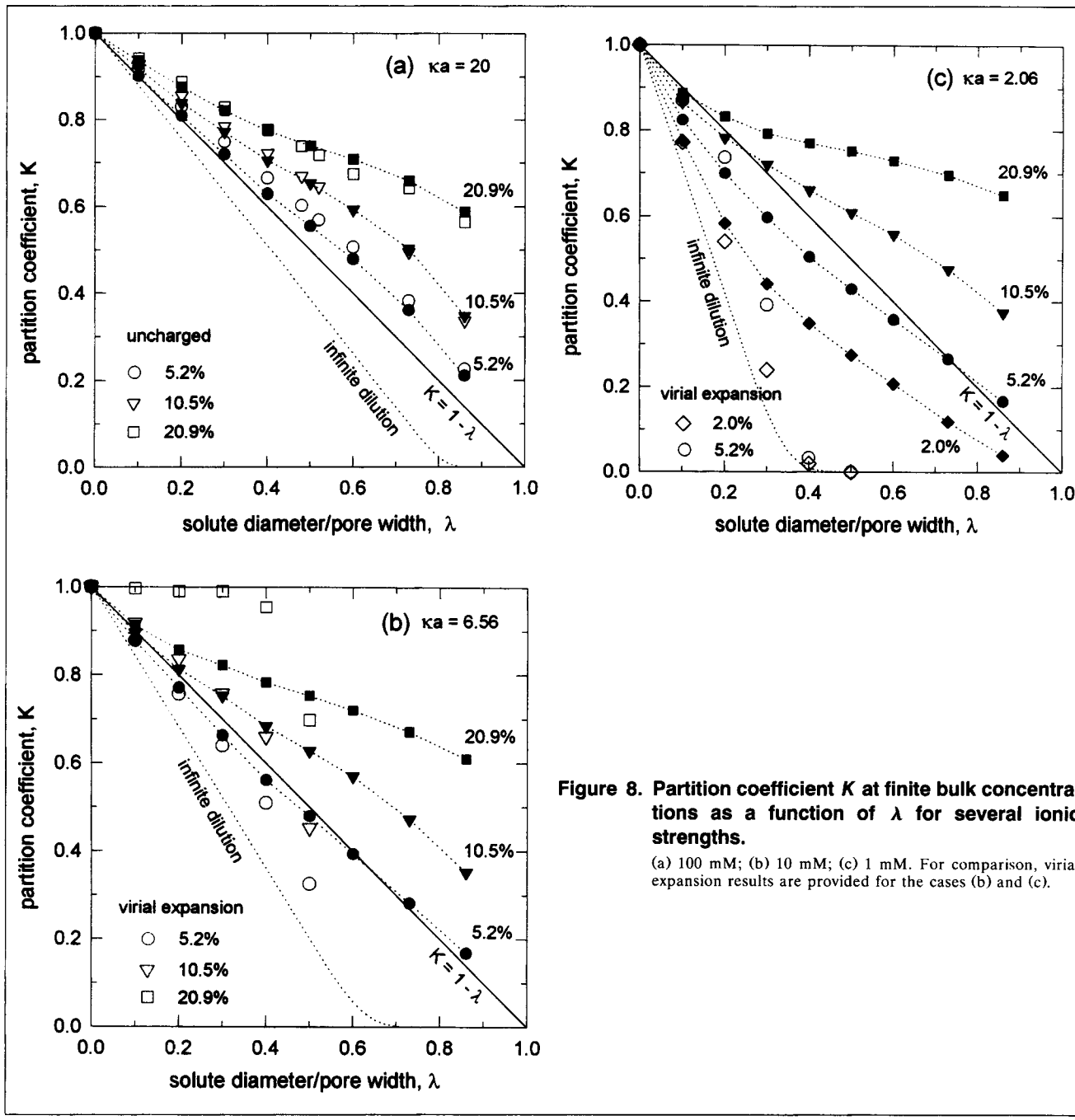

Figure 8. Partition coefficient K at finite bulk concentrations as a function of λ for several ionic strengths.

(a) 100 mM; (b) 10 mM; (c) 1 mM. For comparison, virial expansion results are provided for the cases (b) and (c).

As the thickness of the electrostatic double layer increases, the importance of the repulsive interactions is enhanced. However, since both solute–solute and solute–wall repulsions are affected, the partition coefficient can still become greater than $1-\lambda$ at moderate concentrations between 5 and 10%, depending on the ionic strength. Our results for these cases are shown in Figures 8b and 8c, which correspond to inverse, dimensionless Debye lengths κa of 6.56 and 2.06, respectively. Also shown are results obtained by performing a virial expansion, which are seen to be in good agreement with the simulation results for low concentrations and low values of λ, particularly for small Debye lengths (i.e., large values of κa). The GEMC and virial expansion results agree quantitatively for $\lambda < 0.3$ and $C_b < 10.5\%$ at $\kappa a = 6.56$, and for $\lambda \leq 0.1$ and $C_b < 5.2\%$ at $\kappa a = 2.06$. Numerical values for K_0 and K_1 are given in Table 1. In Figure 8b it is shown that, even at a concentration as low as 5.2%, for $\kappa a = 6.56$ the effect of finite concentration increases K to a value quite close to $1-\lambda$, although still lower than the corresponding value of K for uncharged spheres at a bulk concentration of 5.2%. At an even larger Debye length, corresponding to a value of κa equal to 2.06, the concentration effect is still greater, as seen in Figure 8c: for systems with $\lambda = 0.4$ at infinite dilution the partition coefficient is almost zero, whereas at a bulk concentration of only 5.2% the value of K increases to approximately 0.5.

Table 1. Virial Coefficients for Eq. 17

λ	K_0		K_1	
($= d/D$)	$\kappa a = 6.56$	$\kappa a = 2.06$	$\kappa a = 6.56$	$\kappa a = 2.06$
0.1	0.8398	0.7095	0.7453	3.0958
0.2	0.6797	0.4191	1.4906	6.1050
0.3	0.5235	0.1456	2.2351	4.7243
0.4	0.3620	0.0109	2.8347	0.4351
0.5	0.2030	0.0001	2.3702	0.0026

The effects of solute concentration and ionic strength are shown explicitly in Figures 9 and 10. In Figure 9, values of the partition coefficient K are plotted as a function of bulk concentration C_b for values of λ equal to 0.1 and 0.4. The effect of charge is most pronounced at low solute concentrations, particularly for the narrower slit pore for which $\lambda = 0.4$. Indeed, for $\lambda = 0.4$ at concentrations greater than 20% all the charged results converge on the uncharged result, whereas at infinite dilution the partition coefficient is zero at $\kappa a = 2.06$ and 0.6 for uncharged solutes. The observation that charge effects are reduced at higher solute concentrations is also evident in Figure 10, where it is seen that ionic strength has almost no effect on K for a bulk concentration of 20.9% at $\lambda = 0.4$, and has only a slight effect at $\lambda = 0.1$ at the same concentration.

Figure 11 shows density profiles for charged solutes with bulk concentrations of 5.2% and 20.9% at $\kappa a = 6.56$ in a charged slit pore for which $\lambda = 0.2$. Profiles obtained by the virial expansion method (cf. Eq. 18) are also provided for comparison. The two sets of results are in good agreement at the lower concentration of 5.2%, but do not agree well at 20.9%, because the virial expansion is not accurate at that concentration. The repulsive electrostatic interactions clearly decrease the concentration near the pore wall relative to the uncharged case, which is shown in Figure 6. However, a region of enhanced concentration is also evident, particularly at the higher concentration of 20.9%. Glandt (1980) and Mitchell and Deen (1984) refer to this concentration enhancement as a "shielding" effect owing to the nearby presence of the wall. Comparison with Figure 6 shows that, in a

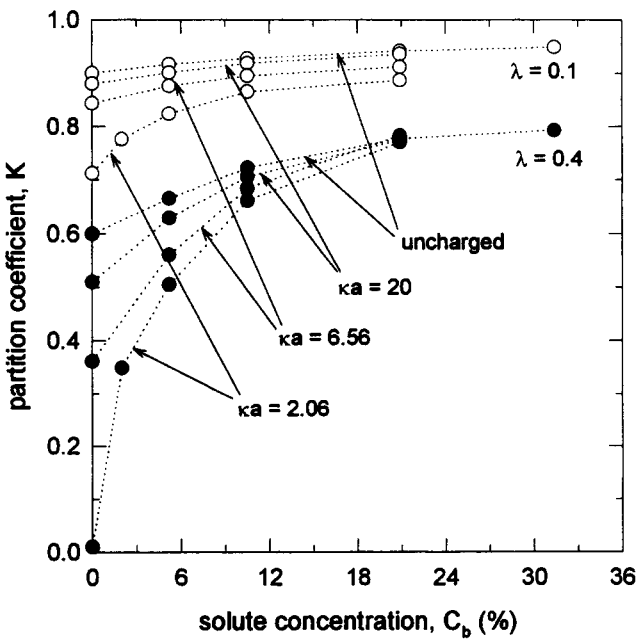

Figure 9. Partition coefficient K as a function of solute concentration at different ionic strengths for $\lambda = 0.1$ and 0.4.

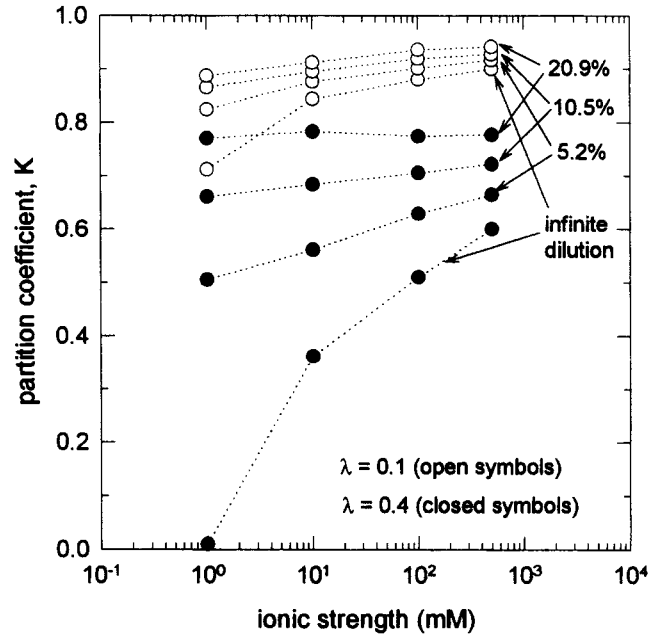

Figure 10. Partition coefficient K as a function of ionic strength for different solute concentrations at $\lambda = 0.1$ and 0.4.

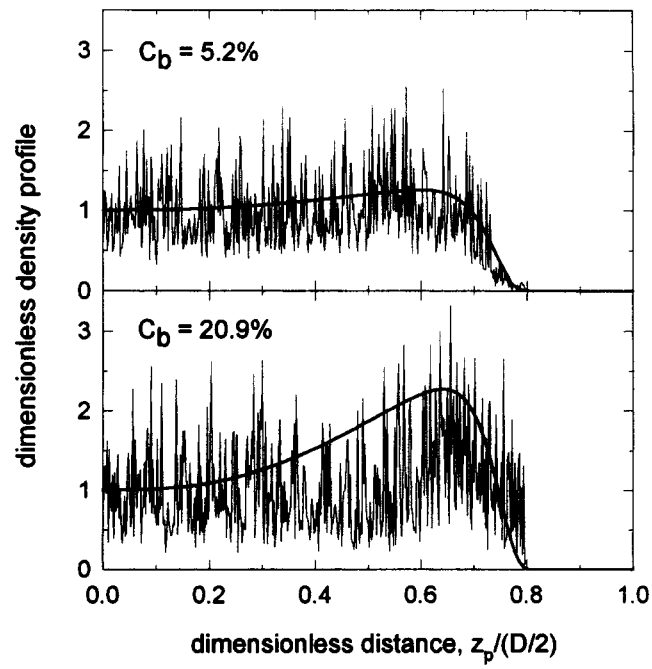

Figure 11. Density profiles of charged solutes in slit pores for $\kappa a = 6.56$, $\lambda = 0.2$ and solute concentrations of 5.2 and 20.9%.

Solid curves correspond to virial expansion results.

qualitative sense, the effect of the electrostatic interaction is to shift this region of enhanced concentration toward the pore center by a distance comparable to the Debye length.

Conclusion

Equilibrium partition coefficients for spherical solutes in slit pores have been calculated by using Gibbs ensemble Monte Carlo simulations. For uncharged systems, our GEMC results compare favorably with results from previous theoretical work obtained by using virial expansions, density functional theory, and the two-dimensional approximation. For very narrow pores, our results indicate that the two-dimensional approximation is more reliable than the other approaches. The presence of electrostatic interactions changes the partitioning behavior significantly, particularly at low solute concentrations. At infinite dilution, repulsive solute–wall electrostatic interactions can dramatically lower the partition coefficient. However, our simulations show that the increase in the partition coefficient caused by finite solute concentration, which is significant even for uncharged systems, is even more so for systems with repulsive electrostatic interactions. Even at bulk concentrations as low as 5.2%, the concentration effect can increase K enough to compensate for the repulsive solute–wall interactions. Hence, for systems at finite solute concentrations, accounting for the concentration effect in predicting partition coefficients should be considered as important as accounting for electrostatic effects.

Acknowledgment

This work was supported by NSF Grant BES-9500663 to RJP. Dr. M.-S. Chun is the recipient of research fellowship from the Korea Science and Engineering Foundation, and acknowledges this support of his overseas study.

Literature Cited

Allen, M. P., and D. J. Tildesley, *Computer Simulation of Liquids*, Oxford Univ. Press, New York (1987).

Anderson, J. L., and J. H. Brannon, "Concentration Dependence of the Distribution Coefficient for Macromolecules in Porous Media," *J. Poly. Sci., Poly. Phys. Ed.*, **19,** 405 (1981).

Carnie, S. L., D. Y. C. Chan, and J. Stankovich, "Computation of Forces between Spherical Colloidal Particles: Nonlinear Poisson-Boltzmann Theory," *J. Colloid Interf. Sci.*, **165,** 116 (1994).

Dabros, T., "A Singularity Method for Calculating Hydrodynamic Forces and Particle Velocities in Low-Reynolds-Number Flows," *J. Fluid Mech.*, **156,** 1 (1985).

de Pablo, J. J., and J. M. Prausnitz, "Phase Equilibria for Fluid Mixtures from Monte-Carlo Simulation," *Fluid Phase Equil.*, **53,** 177 (1989).

Deen, W. M., "Hindered Transport of Large Molecules in Liquid-Filled Pores," *AIChE J.*, **33,** 1409 (1987).

Edwards, S. L., and P. L. Dubin, "pH Effects on Non-ideal Protein Size-Exclusion Chromatography on Superose-6," *J. Chromatog.*, **648,** 3 (1993).

Fanti, L. A., and E. D. Glandt, "Partitioning of Spherical Solutes into Sponge-Type Materials," *AIChE J.*, **35,** 1883 (1989).

Gerald, C. F., and P. O. Wheatley, *Applied Numerical Analysis*, 4th Ed., Addison-Wesley, New York (1992).

Glandt, E. D., "Density Distribution of Hard Spherical Molecules inside Small Pores of Various Shapes," *J. Colloid Interf. Sci.*, **77,** 512 (1980).

Glandt, E. D., "Distribution Equilibrium between a Bulk Phase and Small Pores," *AIChE J.*, **27,** 51 (1981).

Green, D. G., G. Jackson, E. de Miguel, and L. F. Rull, "Vapor-Liquid and Liquid-Liquid Phase Equilibria of Mixtures Containing Square-Well Molecules by Gibbs Ensemble Monte Carlo Simulation," *J. Chem. Phys.*, **101,** 3190 (1994).

Hunter, R. J., *Foundations of Colloid Science*, Vol. 1, Clarendon Press, Oxford (1989).

Lastoskie, C., K. E. Gubbins, and N. Quirke, "Pore Size Heterogeneity and the Carbon Slit Pore: A Density Functional Theory Model," *Langmuir*, **9,** 2693 (1993).

Lozada-Cassou, M., and E. Diaz-Herrera, "Three Point Extension for Hypernetted Chain and Other Integral Equation Theories: Numerical Results," *J. Chem. Phys.*, **92,** 1194 (1990a).

Lozada-Cassou, M., and E. Diaz-Herrera, "Three Point Extension Hypernetted Chain, Conventional Hypernetted Chain, and Superposition Approximations: Numerical Results for the Force between Two Plates," *J. Chem. Phys.*, **93,** 1386 (1990b).

MacElroy, J. M. D., and S.-H. Suh, "Concentration and Non-continuum Effects in Size-Exclusion Partitioning," *AIChE Symp. Ser.*, **82**(248), 133 (1986).

MacElroy, J. M. D., and S.-H. Suh, "Computer Simulation of Moderately Dense Hard-sphere Fluids and Mixtures in Microcapillaries," *Mol. Phys.*, **60,** 475 (1987).

Mitchell, B. D., and W. M. Deen, "Theoretical Effects of Macromolecule Concentration and Charge on Membrane Rejection Coefficients," *J. Memb. Sci.*, **19,** 75 (1984).

Panagiotopoulos, A. Z., "Direct Determination of Phase Coexistence Properties of Fluids by Monte Carlo Simulation in a New Ensemble," *Mol. Phys.*, **61,** 813 (1987).

Panagiotopoulos, A. Z., N. Quirke, M. Stapleton, and D. J. Tildesley, "Phase Equilibria by Simulation in the Gibbs Ensemble: Alternative Derivation, Generalization and Application to Mixture and Membrane Equilibria," *Mol. Phys.*, **63,** 527 (1988).

Phillips, R. J., "Calculation of Multisphere Linearized Poisson-Boltzmann Interactions near Cylindrical Fibers and Planar Surfaces," *J. Colloid Interface Sci.*, **175,** 386 (1995).

Pospisil, R., A. Malijevsky, and P. Jech, "Integral Equation and Computer Simulation Studies of Hard Spheres in a Slit Pore," *Mol. Phys.*, **78,** 1461 (1993).

Post, A. J., "Solute Partitioning between a Micropore and a Bulk Solution: A Linear Density Functional Approach," *J. Colloid Interf. Sci.*, **129,** 451 (1989).

Post, A. J., and D. A. Kofke, "Fluids Confined to Narrow Pores: A Low-Dimensional Approach," *Phys. Rev. A*, **45,** 939 (1992).

Smith, F. G., and W. M. Deen, "Electrostatic Effects on the Partitioning of Spherical Colloids between Dilute Bulk Solution and Cylindrical Pores," *J. Colloid Interf. Sci.*, **91,** 571 (1983).

Yau, W. W., J. J. Kirkland, and D. D. Bly, *Modern Size-Exclusion Liquid Chromatography*, Wiley, New York (1979).

Manuscript received July 26, 1996, and revision received Dec. 26, 1996.